UR-NCUR 13-031

THE UNIVERSITY OF ROCHESTER

Nuclear Science Research Group

ROCHESTER, NEW YORK 14267-0216, USA

Radioluminescent Characteristics of the EJ 299-33 Plastic Scintillator

S. Nyibule, E. Henry, W. U. Schröder, J. Tõke, L. Acosta, L. Auditore, G. Cardella, E. DeFilippo, L. Francalanza, S. Gianni, T. Minniti, E. Morgana, E. V. Pagano, S. Pirrone, G. Politi, L. Quattrocchi, F. Rizzo, P. Russotto, A. Trifiro, M. Trimarchi

April 2013 (Submitted to Nuclear Instruments and Methods for Physics Research A)

Radioluminescent Characteristics of the EJ 299-33 Plastic Scintillator

S. Nyibule[a], E. Henry[a], W.U. Schröder[a,b], J. Tõke[a], L. Acosta[c,g], L. Auditore[d], G. Cardella[e], E. DeFilippo[e], L. Francalanza[f,c], S. Gianni[f], T. Minniti[d], E. Morgana[d], E. V. Pagano[f,c], S. Pirrone[e], G. Politi[e,f], L. Quattrocchi[d], F. Rizzo[f,1], P. Russotto[e], A. Trifiro[d], M. Trimarchi[d]

[a] *University of Rochester, Department of Chemistry, Rochester, NY 14627, USA*
[b] *University of Rochester, Department of Physics, Rochester, NY 14627, USA*
[c] *Instituto Nazionale di Fisica Nucleare, Laboratori Nazionali del Sud, Catania, Italy*
[d] *Instituto Nazionale di Fisica Nucleare, Gruppo Collegato di Messina and Department of Physics, Messina University, Messina, Italy*
[e] *Instituto Nazionale di Fisica Nucleare, Sezione di Catania, Italy*
[f] *Department of Physics and Astronomy, Catania University, Catania Italy*
[g] *Departamento de Fisica Aplicada,Universidad de Huelva, Huelva, Spain*

Abstract

The response of the EJ 299-33 plastic scintillator to energetic charged nuclear particles ranging from isotopes of hydrogen to isotopes of carbon has been determined over a wide energy range using a complex experimental setup and nuclear reactions induced by a 20 AMeV carbon beam on an aluminum target. A strong pulse-shape dependence of the generated light bursts on the impinging particle specie is observed, which makes this scintillator suitable, among other things, for neutron *vs.* γ-ray identification. Fit formulas are proposed for the normalized light output as a function of particle energy for eleven isotopes of elements ranging from hydrogen to carbon.

Keywords: Plastic scintillators, Pulse-shape discrimination

1. Introduction

Plastic scintillators play important role in the detection of nuclear radiation [1] since the dawn of nuclear research. They have several beneficial properties including the ease of machining and a relatively low cost per volume, which makes them useful in many practical applications. However, unlike select liquid or crystallic scintillators, until recently, they lacked the pulse-shape discrimination capability needed in the applications where neutrons are to be measured in the presence of γ radiation. The latter drawback is now gone with a commercial release of a new type of plastic scintillator by Eljen Technology [3] named EJ 299-33,[2] inviting its use in nuclear science experimentation.

The present study is a part of a broader exploration into the feasibility of using the EJ 299-33 plastic in multi-detector arrays, with the purpose of extending the conventional charged-particle-identification capabilities of the latter by the highly desired capability of identifying neutrons in the presence of γ and charged-particle radiation and of actually measuring their energy spectra. It aims first, at identifying the impinging radiation and measuring its energy and then, at determining the light output produced by this radiation as a function of particle specie and energy. To achieve this goal, additionally, large area silicon transmission detectors were used in a setup allowing also for an independent measurement of particle velocities using the time of flight methodology.

The present paper is constructed as follows: in Section 2 the relevant details of the experimental setup are described, including its salient mechanical, electronics, and data acquisition essentials. Section 3 presents the experimen-

tal results, both raw and refined, and Section 4 presents the summary and discussion.

2. Experimental Methodology

The experiment was performed at the cyclotron facility of Laboratori Nazionali del Sud in Catania, Italy. As illustrated in Fig.1, a pulsed beam of 20 AMeV ^{12}C ions bombarded a 164-μg/cm^2 ^{27}Al target located at the operational center of a reaction chamber. The detector telescope, including the EJ 299-33 scintillator of interest was placed at approximately 1.2 m from the target at an angle of approximately 5°. The telescope consisted of two two-sided large-area multi-strip silicon transmission detectors, followed by the scintillation detector assembly. Both silicon detectors were approximately 400 μm thick and had identical shape of a 60° sector of an annular entity with an inner radius of 5 cm and a outer radius of 2 cm. They featured 16 equally spaced concentric strips on one side and 8 radial sectors on the other.

The scintillation detector assembly consisted of a 5 cm by 5 cm cylindrical EJ 299-33 plastic, optically coupled to the photocathode of a Hamamatsu R7724 photomultiplier tube of spectral response range from 300 to 650 nm, all operated under high vacuum. The photomultiplier tube was operated at 2kV of anode voltage supplied via a base model VD23N-774, also by Eljen Technology.[3] The latter base was passively cooled via a 3-cm wide woven copper ribbon thermally coupled to the massive aluminum structure of the reaction chamber. The temperature of the phototube base was monitored and found to stabilize around 30° on the Celsius scale.

Each of the 48 strips of the two silicon detectors was handled by its

individual electronic channel consisting of a charge-integrating preamplifier, a constant fraction discriminator (CFD), an analog to digital converter (ADC), and a time to digital converter (TDC). The common start signal for the time-of-flight measurement was provided by the cyclotron RF frequency, prescaled and synchronized to the 120-ns micro-structure of the beam. The stop signals were then provided by the CFDs of the individual strips.

The anode signal of the Hamamatsu phototube was fed to three electronic channels for the purpose of time-of-flight measurement and for the purpose of measuring the light output over two different time periods, respectively. The first of these channels was subsequently handled by a TDC, while the latter two channels were handled by two charge-integrating ADCs (QDCs). One of the latter channels was set up to integrate the full extent of the signal and the other one to cover only the "tail" portion of the signal, starting approximately 50 ns after the CFD signal. The settings of the two gates are illustrated in Fig. 2 along with a typical waveform of the phototube anode signal. To satisfy the timing conditions for the QDCs, the anode signals in the two latter channels were delayed by approximately 200 ns using timing-grade (low dispersion) concentric cables of suitable lengths. Note that the two QDC channels were set up with gating signals optimized so as to utilize the pulse-shape discrimination capability of the EJ 299-33 plastic.

In total, the attached data acquisition system digitized and recorded xxx signals of importance for the present study.

3. Experimental Results

A selection of experimental results relevant to the present study is shown in Figs. 3 - 5 and in Table 1, with the first two of the figures documenting intermediate steps leading to the main results presented in Fig 5 and in said table.

Fig. 3 illustrates a typical particle identification plot in a conventional $\Delta Evs.E$ representation, with the former derived from the second silicon detector and the latter representing the normalized light output of the EJ 299-33 scintillation detector. The light output is normalized to that produced by electrons, and effectively, the reaction γ - rays and, hence, expressed in units of electron-equivalent mega electron volts. This abscissa quantity is obviously related to the total energy deposit by a particle in the scintillator material, with the detailed relationship being the very aim of the present study. As sen in Fig. 3, one is able to identify 11 individual species of particles as having statistics sufficient for a quantitative analysis. The domain of hydrogen isotopes could be further expanded in the course of the analysis for a reliable separation of individual ridges for protons, deuterons, and tritons.

To improve on the background handling, the present analysis relied further on a pulse-shape discrimination of signals from light charged particles and neutrons, with the latter being indistinguishable from protons. The particle ID signal PID was in this case derived form the ratio of the fractional charge extracted from the anode of the EJ 299-33 detector assembly to the total charge, using the dual-gating method as described in Section 2 according to

$$PID = \frac{Q_{tail} - pedestal_{tail}}{Q_{total} - pedestal_{total}}, \quad (1)$$

where the two pedestal values for the two QDC channels involved were determined from the response of these respective channels to a zero signal. Note, that of the two pedestals, only the latter is of importance as far as the quality of the particle identification is involved.

One notes in Fig. 4 a very good separation of intensity ridges due to γ-rays, on the one hand and protons, on the other. This quality is what distinguishes the EJ 299-33 plastic scintillator from other plastic scintillators and is a welcome characteristics from the point of view of neutron detection and identification.

The main results of the study are displayed in Fig. 5 and in Table 1. Fig. 5 illustrates the dependence of the light output of the EJ 299-33 scintillator on the kinetic energy and the specie of an impinging particle. The light output function $L(E)$ is here expressed in units of electron-equivalent mega electron volts MeV_{ee}, and is well approximated by quadratic in particle energy E function over a wide energy range, up to that of the ^{12}C beam energy of 20 AMeV. The quadratic fit curves are shown in Fig. 5 in the form of solid lines. The fit function is expressed as:

$$L(E, Z, A) = c_o(Z, A) + c_1(Z, A)E + c_2(Z, A)E^2, \quad (2)$$

where the coefficient $c_o(Z, A)$, $c_1(Z, A)$, and $c_2(Z, A)$ are treated as fit parameters for individual particle species identifies by their atomic and mass numbers Z and A, respectively. Note that, as pointed out in Section 2, the true particle energy was determined based on the time-of-flight measurement

with respect to the cyclotron RF signal and the particle ID determined based on the techniques discussed further above.

Table 1 shows the values of the best χ-square fit parameters for the 11 isotopes for which the identification was possible based on the limited statistics collected in the present test experiment. One must note that the non-zero value of $c_o(Z, A)$ reflects solely the accuracy of the fit in a χ-square search routine and that the data points at very low energies may have systematic accuracies beyond the statistical ones included in this routine. Given the overall quality of the fit, one may find it well justified to extrapolate the measured light output functions well beyond the domain covered in the present experiment.

4. Summary

The on-beam study of the radioluminescent characteristics of the EJ 299-33 plastic scintillator have confirmed its potential value to the nuclear engineering and science community in its unique among plastic scintillators dependence of the waveform of the light pulse on the type of nuclear radiation that gave rise to this pulse. With the specific and more focussed aim of the present study, light output functions have been measured over a range of particle energies of up to 20 AMeV. A simple quadratic parametrization was shown to fit these experimental functions in a fashion suggesting that an extrapolation of such a parametrization over a significant energy range may be meaningful.

Further evaluations of the utility of the EJ 299-33 plastic in the environment of large reaction chambers, "stuffed" with multi-detector arrays are

in progress, based on the full set of experimental data gathered in the experiment considered in the present study. Their findings will be published promptly in separate papers.

This work was supported by the U.S. Department of Energy grant No. DE-FG02-88ER40414.

References

[1] G. Knoll, *Radiation Detection and Measurement* John Wiley & Sons, Inc (2000).

[2] N. Zaitseva *et al.*, Nucl. Instr. and Meth. Phys. Res. A **668** 88 (2012).

[3] Eljen Technology, http://www.eljentechnology.com/

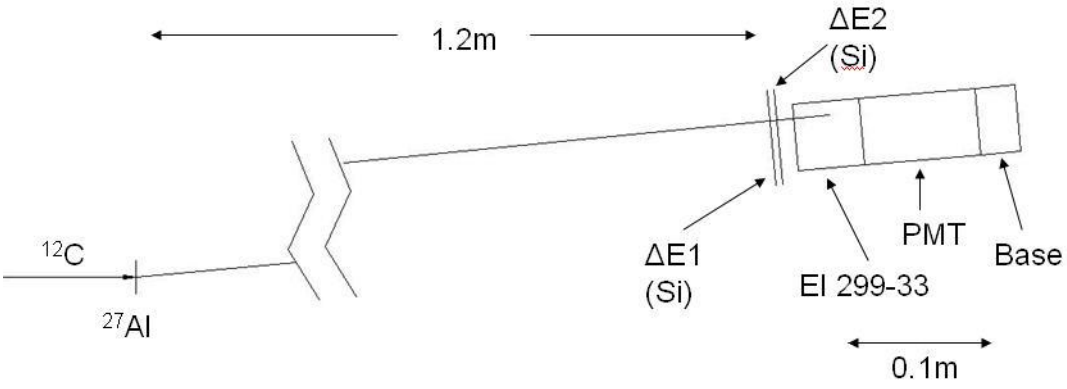

Figure 1: A schematic view of the experimental setup, showing two spatial domains with borders indicated by vertical zig-zag lines. (See text.)

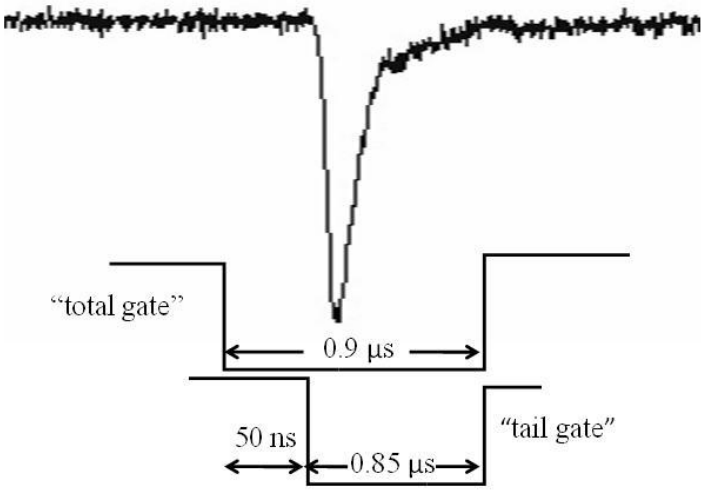

Figure 2: Schematic depiction of a temporal relationship between the PMT signal and the two gates - "total" and "tail", used in the pulse-discrimination routine.

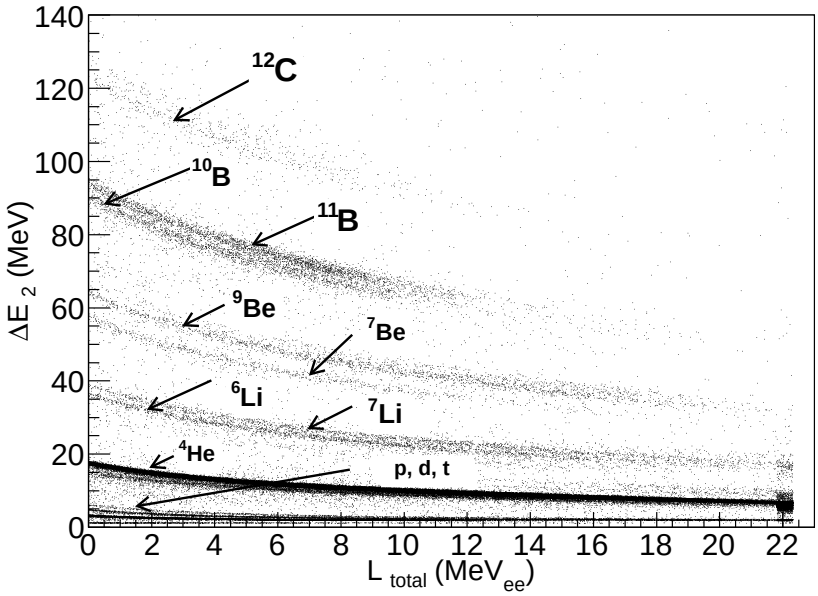

Figure 3: Particle identification patters for 11 isotopes ranging from hydrogen to carbon. Plotted are the total light output in units of electron-equivalent MeV (abscissa) and the energy lost by the particle in the second transmission silicon detector ΔE (ordinate).

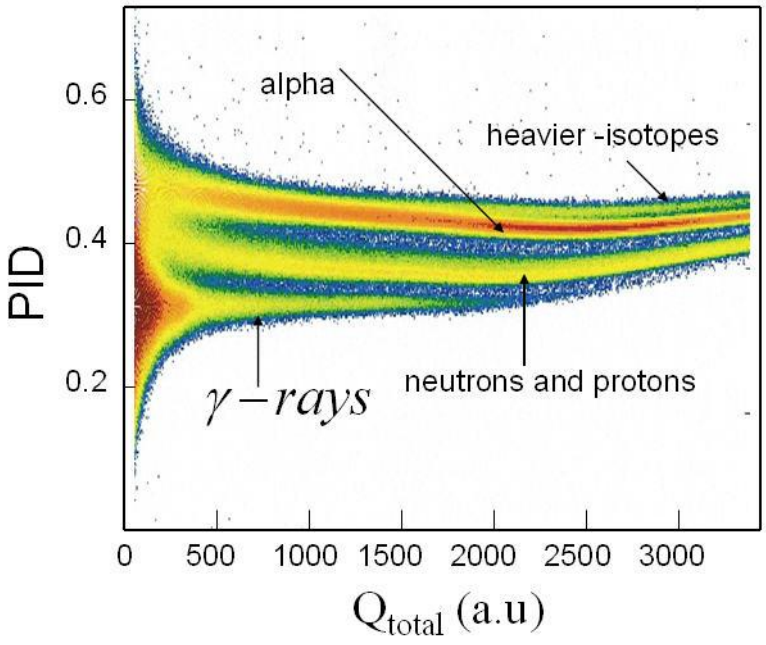

Figure 4: (Color online) Pulse shape discrimination pattern for γ-rays, protons, α- particles and heavier fragments obtained using a conventional two-gate, two-channel QDC measurement (see Fig. 2) as applied to the the anode signals of the EJ 299-33 scintillation detector. Plotted on the ordinate axis is the PID signal derived from the two portions of the charge, *total* and *tail*, extracted from the anode of the EJ 299-33 detector assembly. (See text.)

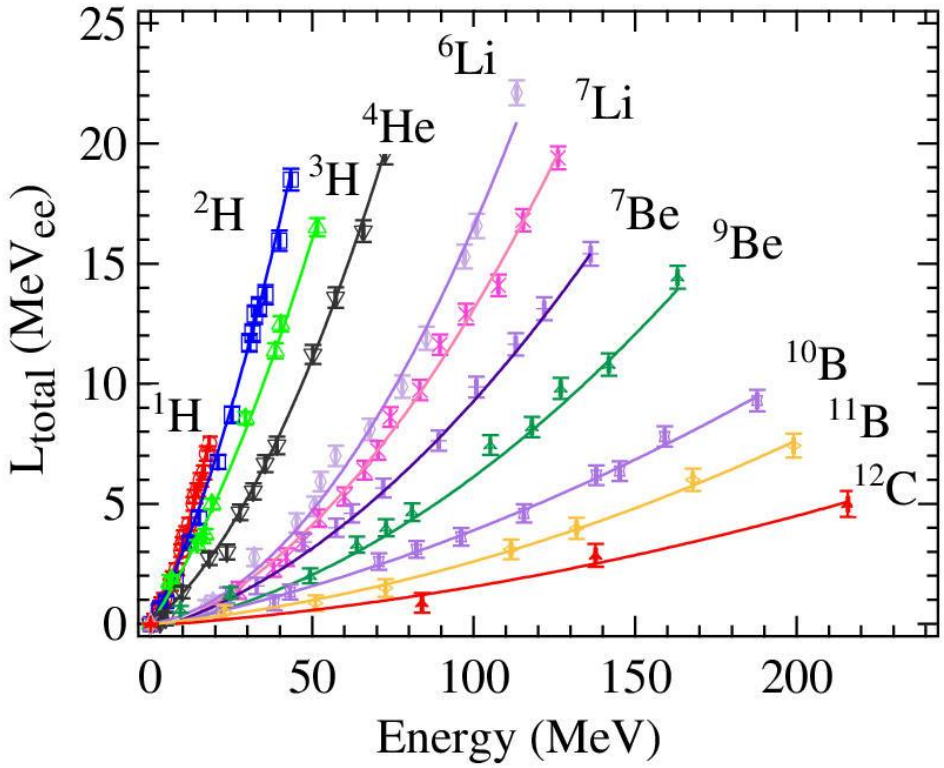

Figure 5: (Color online) Light output functions for various isotopes of elements ranging from hydrogen to carbon. Symbols represent experimental points, while the solid curves represent the respective fit functions of Eq 2, as evaluated using the parameters listed in Table 1.

Table 1: Fit parameters obtained by fitting a quadratic function of the form given by Eq. 2 to the light output functions for different species of particles, as seen in Fig. 2.

Particle	c_o	c_1	c_2*1000
p	-0.15 ± 0.1	0.25 ± 0.03	9.6 ± 1
d	-0.27 ± 0.2	0.26 ± 0.02	3.9 ± 0.5
t	0.09 ± 0.3	0.21 ± 0.03	2.2 ± 0.5
^{4}He	-0.14 ± 0.1	0.11 ± 0.01	2.2 ± 0.1
^{6}Li	0.15 ± 0.5	0.023 ± 0.02	1.4 ± 0.1
^{7}Li	-0.38 ± 0.4	0.045 ± 0.01	0.9 ± 0.05
^{7}Be	-0.08 ± 0.2	0.041 ± 0.01	0.5 ± 0.04
^{9}Be	0.17 ± 0.2	0.036 ± 0.01	0.37 ± 0.05
^{10}B	-0.13 ± 0.1	0.028 ± 0.004	0.12 ± 0.02
^{11}B	-0.02 ± 0.1	0.014 ± 0.003	0.12 ± 0.05
^{12}C	-0.08 ± 0.5	0.010 ± 0.01	0.06 ± 0.04